https://doi.org/10.5194/essd-2026-135
Preprint. Discussion started: 28 April 2026

Open Access Earth System Science Data Discussions

Dataset of airborne measurements of aerosol, cloud droplets and meteorology by tethered balloon during PaCE 2022

Viet Le[1], Konstantinos Doulgeris[1], Mika Komppula[1], John Backman[1], Gholamhossein Bagheri[2], Eberhard Bodenschatz[2], and David Brus[1]

[1]Finnish Meteorological Institute, Helsinki, FI-00560, Finland
[2]Max Planck Institute for Dynamics and Self-Organization, Am Fassberg 17, 37077 Göttingen, Germany

Correspondence: Viet Le (viet.le@fmi.fi)

Abstract.

Aerosol, cloud droplet, and meteorological measurements were carried out by the Finnish Meteorological Institute's payload onboard the tethered balloon systems during the Pallas Cloud Experiment 2022 in Finland. This dataset includes 21 flights between September 16th and October 10th. The observations include vertical profiles and time series of aerosol number concentration and size distribution; cloud droplet number concentration and size distribution; and meteorological parameters. This dataset has been uploaded to the common Zenodo PaCE 2022 community archive (https://zenodo.org/communities/pace2022/, last access: Jan 20, 2025). This dataset (Le et al., 2026) is available at: https://doi.org/10.5281/zenodo.14932881.

1 Background

The most pronounced impact of climate change is in the Arctic region, where the warming is nearly four times as large as the global average (Rantanen et al., 2022). This phenomenon is known as Arctic amplification and has been observed in paleoproxy reconstruction of past climate (Park et al., 2019), present-day instrumental observations (Bekryaev et al., 2010; Esau et al., 2023), and future predictions of climate models (Holland and Bitz, 2003; Davy and Outten, 2020). It is projected that Arctic sea ice during summers will completely melt by 2050 (Ono et al., 2022), leading to the disruption of Arctic ecosystems and inhabitants, as well as significant alterations to global climate patterns.

Early research has linked Arctic amplification to the sea ice albedo feedback (Manabe and Wetherald, 1975), which is a positive feedback that accelerates sea ice melting through the decrease of surface albedo due to sea ice loss. Additionally, this loss of sea ice destabilizes the boundary layer and enhances moisture availability and boundary layer convection (Kay and Gettelman, 2009; Vavrus et al., 2009; Philipp et al., 2020). As a result, there is an increase in Arctic low clouds in fall and winter as observed in recent decades (Cao et al., 2017; Philipp et al., 2020). Given the impact of clouds on the global radiation budget, many studies (Vavrus, 2004; Taylor et al., 2013) have confirmed the importance of cloud feedback in Arctic amplification. These abundant Arctic low-level clouds can exert a warming effect, particularly outside the summer season, by enhancing downward longwave radiation (Taylor et al., 2013; Cao et al., 2017). This process accelerates sea ice melt and

https://doi.org/10.5194/essd-2026-135
Preprint. Discussion started: 28 April 2026

increases atmospheric moisture, which promotes the formation of liquid clouds over newly exposed open water (Kay et al., 2016; Tan and Storelvmo, 2019; Huang et al., 2021). This positive feedback further enhances downward longwave radiation.

Currently, the uncertainty of Arctic cloud feedback remains high in climate models (Forster et al., 2021). A major factor contributing to this issue is the lack of reliable observations of aerosols and clouds. Aerosols can serve as cloud condensation nuclei (Aitken, 1881), playing a crucial role in cloud formation and influencing cloud properties. Dada et al. (2022) and Doulgeris et al. (2023) demonstrated that anthropogenic pollution has a significant impact on cloud properties, especially in Arctic and sub-Arctic clean environments. The increase in anthropogenic pollution leads to a higher cloud condensation nuclei concentration, which subsequently increases the cloud droplet number concentration (N_d), e.g. Twomey (1959). As a result, the effective diameter (ED) of the cloud droplets decreases, altering the cloud's radiative properties by increasing its albedo. The resulting enhancement of shortwave cooling can offset the longwave warming effect of clouds, thereby weakening the cloud–ice warming feedback, particularly during autumn (Kay et al., 2016). Moreover, small cloud droplets also inhibit precipitation and prolong cloud lifetime, which ultimately enhances the cloud's liquid water content (LWC). Despite the well-known impact of aerosols on cloud properties, quantifying the aerosol-cloud interaction (ACI) remains highly uncertain, with only a slight reduction in uncertainty across the past six IPCC reports (Forster et al., 2021). As a result, accurate observations of aerosols and clouds are essential for enhancing our understanding of this interaction.

In the last three decades, airborne missions utilizing large crewed aircraft have yielded valuable information on aerosols and their impact on cloud microphysics over the Arctic (Curry et al., 1988; Borys, 1989; Browell et al., 1992; Lathem et al., 2013; Ancellet et al., 2014; Abbatt et al., 2019). However, they are logistically and financially demanding, making them only feasible for large-scale campaigns. Moreover, they are often not able to fly within hundreds of meters above the surface, preventing them from measuring the often low-level clouds in the Arctic. Tethered balloon systems (TBS) are gaining recognition as a valuable platform for collecting vertical distribution of aerosols and clouds in recent years (Hara et al., 2013; Ferrero et al., 2019; Creamean et al., 2021; Pohorsky et al., 2024a). It offers distinct advantages and limitations related to flight ceiling, profiling, cost, and payload capacity. However, a key benefit of TBS is its ability to profile and remain stationary at specific altitudes, even inside clouds, with flight durations of several hours possible, depending on the power available for instrumentation.

In this paper, we present our collected aerosol, cloud and meteorological measurements onboard a TBS during the Pallas Cloud Experiments (PaCE) campaign in 2022. The campaign was conducted in Pallas, northern Finland, from September 16th to October 10th, 2022, and is part of the ongoing PaCE campaigns that have been running for two decades (Doulgeris et al., 2022). In the following sections, we provide an overview of the campaign, instruments, and dataset measured by the FMI's payload. These observations are crucial for identifying key processes related to aerosol and cloud interactions. Additionally, they provide an important observational basis for models, ground-based remote sensing, and satellite data validation.

2 Campaign overview

Over the last two decades, the Finnish Meteorological Institute (FMI) has carried out PaCE campaigns in the subarctic region of Finnish Lapland. These campaigns played a key role in providing extensive observations for clouds and aerosols research in

https://doi.org/10.5194/essd-2026-135
Preprint. Discussion started: 28 April 2026

Open Access Earth System Science Data Discussions

the Arctic (Komppula et al., 2005; Lihavainen et al., 2010; Doulgeris et al., 2020, 2022). In 2022, PaCE was held once again in Pallas, Finland (Figure 1), with participation from several institutes across Europe, each deploying different instrumentation and measurement platforms. The objective of the campaign is to collect high resolution vertical atmospheric data in the vicinity of the Global Atmospheric Watch (GAW) Sammaltunturi station, which is located approximately 295 m above the balloon launch site and about 160 km north of the Arctic Circle (Doulgeris et al., 2022). The campaign utilized a variety of methods to gather comprehensive datasets on atmospheric properties, such as airborne in-situ measurements onboard uncrewed aerial systems (UAS) and TBS, as well as ground-based in-situ and remote sensing observations. This was the first use of airborne in-situ measurements onboard TBS in PaCE.

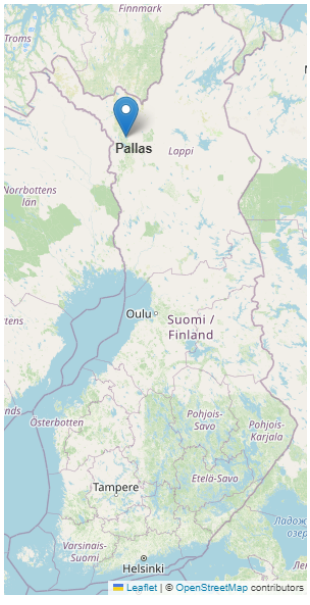

Figure 1. Location of PaCE 2022 campaign in Pallas, Lapland, northern Finland. © OpenStreetMap contributors, https://www.openstreetmap.org/copyright.

The data presented in this paper was measured by a FMI's payload onboard TBSs during the intensive part of the campaign, from September 16th to October 10th, 2022. During the first two weeks from September 16th to September 28th, the FMI's payload was onboard the Max Planck CloudKite (MPCK) platform (see Fig. 2a) operated by the Max Planck Institute for Dynamics and Self-Organization (Chávez-Medina et al., 2025; Schlenczek et al., 2025). The MPCK platform was flown during the PACE campaign in a tandem configuration, i.e. a 250 m^3 helikite with a 34 m^3 helikite above it (both Desert Star Helikites Allsopp Helikites Ltd.). These helikites, which are hybrids of helium balloons and kites, have stable flight behaviour in both calm and windy conditions with a maximum payload of up to 100 kg at 1 km above sea level. The flight altitude of the MPCK platforms can be controlled by reeling in and out the tether with a gasoline winch. This unintentionally resulted in the measurements being affected by gasoline emissions, as discussed in the next Section below.

https://doi.org/10.5194/essd-2026-135
Preprint. Discussion started: 28 April 2026

Starting from September 29th, FMI's payload was onboard FMI's tethered balloon system Aerostat by SkyDoc Systems Inc. (see Fig. 2b). The Aerostat system consists of a tethered balloon, a winch, and a tether line (about 1 km in length), which is controlled by the winch. Unlike the MPCK platform, the Aerostat is operated by using an electric winch, ensuring no interference with the payload measurements. When inflated with 50 m^3 helium, the Aerostat provides a net lift capacity of approximately 37 kg under zero wind conditions at sea level. The FMI payload had a weight of about 8 kg and contained several instruments designed to measure meteorological parameters, as well as properties of cloud and aerosol particles. A detailed description of these instruments will be provided in the next section.

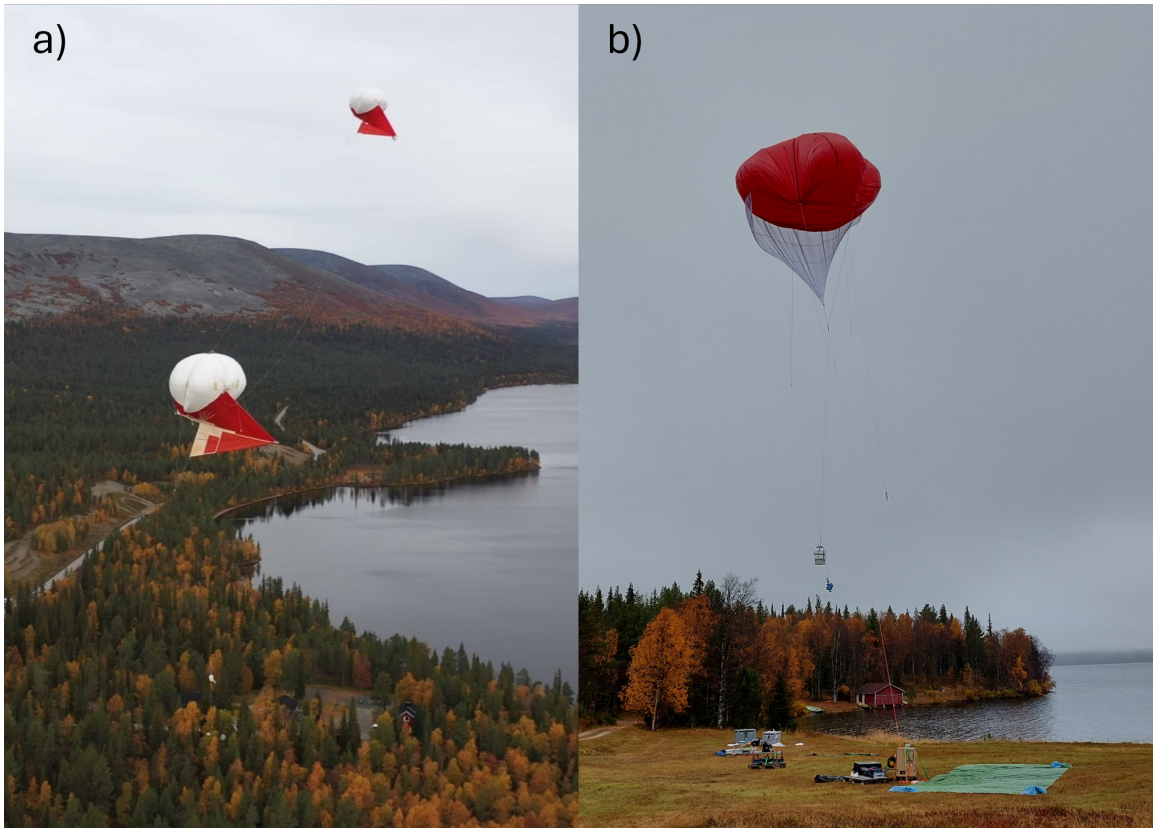

Figure 2. FMI's payload onboard a) the MPCK platform, b) the FMI's TBS (Aerostat, SkyDoc Systems Inc.).

Both the MPCK platform and Aerostat were launched at the Pallasjärvi lake beach (68°01'23.2"N, 24°09'48.8"E), with the launch site situated at an elevation of 276 meters above sea level. The site has minimal local traffic with the main road being located approximately 500 m away. During the usual flights, the maximum horizontal distance of the MPCK platform and Aerostat from the launch site was around 700 m, and their maximum height above ground level was up to 1.5 km. During the measurement period, the weather was mild. The temperature measured by the payload ranged from -1 to 6 °C, which minimized ice collection on the surfaces that could also lead to clogging of the instruments' inlets. The wind was moderate for

https://doi.org/10.5194/essd-2026-135
Preprint. Discussion started: 28 April 2026

most of the measurement period, averaging at approximately 6.8 $\mathrm{m\,s^{-1}}$ (measured at Sammaltunturi station, Backman et al. (2025)). Several flying schemes have been utilized during the campaign, such as stationary sampling at the altitude of the cloud layer or vertical profiling.

On October 10th, an unexpected incident occurred during the TBS operation. A sudden gust of wind caused the balloon's tethered line to snap, allowing the balloon and its payload to drift away freely. The balloon ascended to an altitude of 8 km before bursting, after which it descended and landed in a forest. The payload remained fully operational, and all data were successfully recorded. Analysis of the recovered data showed that the balloon ascended at approximately 4–5 $\mathrm{m\,s^{-1}}$ and descended at 3–4 $\mathrm{m\,s^{-1}}$, while its horizontal speed varied between 5 and 15 $\mathrm{m\,s^{-1}}$. It traveled a total distance of 50 km in 1 hour and 17 minutes. A small hole was found in the balloon afterwards, indicating that it burst at 8 km altitude and then slowly descended as helium leaked, behaving like a parachute and reaching a terminal velocity of about 4 $\mathrm{m\,s^{-1}}$. This event provided a unique dataset and highlighted important lessons for balloon flight safety, including regular tethered line inspections, gust-forecast checks, redundant safety lines, use of pulleys to maintain perpendicular alignment with the winch drum, and measures to prevent tethered line damage from sudden wind shifts.

https://doi.org/10.5194/essd-2026-135
Preprint. Discussion started: 28 April 2026

3 Instrument overview and quality control

FMI built a custom battery-powered payload consisting of multiple instruments (Fig. 3) to measure the aerosol, cloud droplets and basic meteorological conditions. The payload complements other concurrent airborne observations conducted during the campaign, including atmospheric boundary layer wind turbulence (Chávez-Medina et al., 2025) and cloud microphysics (Schlenczek et al., 2025). The payload had overall dimensions of 32 × 40 × 100 cm (length × width × height). It was suspended beneath the balloon on a 4 m line and equipped with a directional stabilizer. The stabilizer consisted of a 3 m line with a wind-inflated plastic bag attached, designed to minimize payload rotation (see Fig. 2b). A detailed analysis of sampling losses for all instruments due to potential payload rotation and wind speed is presented in Section S1 of the Supplement.

The payload consisted of a basic meteorological sensor (BME 280, Bosch Sensortec), a condensation particle counter (CPC, model 3007, TSI Inc.), a portable optical particle spectrometer (POPS, Handix Inc.), and a prototype of a mini cloud droplet analyzer (mCDA, Palas GmbH). All the data were logged by a Raspberry Pi 3+ minicomputer using Python scripts to ensure that the time stamps were synchronized. The BME, CPC, and POPS were logged at a rate of 1 Hz, while mCDA was logged at a rate of 10 Hz. The Raspberry Pi, CPC, and their batteries were placed inside a styrofoam box with the wall thickness of 2.5 cm, while the remaining instruments were housed in their own enclosures and attached to the outside of the styrofoam box. This ensures optimal operating temperature for all instruments. The thermal insulation of the instruments is discussed below and in the Supplement.

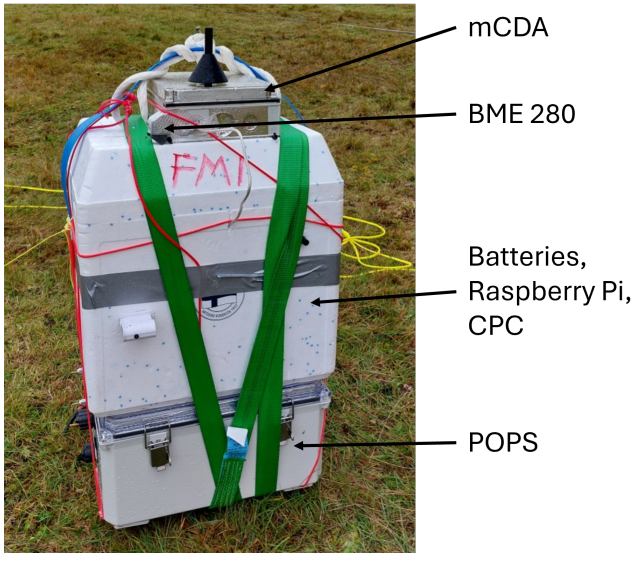

Figure 3. The FMI payload.

The BME sensor (BME 280, Bosch Sensortec) (Brus et al., 2021; Pilz et al., 2022) was used to measure ambient conditions outside the payload, including pressure (p), temperature (T), and relative humidity (RH). The BME sensor has a manufacturer-stated accuracy (at 25°C) of ±1 hPa for p, ±0.5°C for T, and ±3 % for RH (Humidity sensor BME 280: https://www.bosch-

https://doi.org/10.5194/essd-2026-135
Preprint. Discussion started: 28 April 2026

sensortec.com/products/environmental-sensors/humidity-sensors-bme280/, last access: 08 December 2024). The BME sensor was placed inside a perforated plastic housing and shielded from solar radiation. An intercomparison between in-flight BME measurements and the reference Vaisala Automatic Weather Station at Sammaltunturi, selected at the same height within ±40 m is shown in Section S2 of the Supplement. The results indicate a strong correlation in temperature measurement ($p < 0.05$, $R^2 = 0.88$), and a linear regression slope of 0.913. For the relative humidity, the BME sensor reports values approximately 5 to 10% lower than the reference measurements, consistent with findings reported by Barbieri et al. (2019) for various small UAS platforms.

The CPC (CPC, model 3007, TSI Inc.) (Hämeri et al., 2002; Mordas et al., 2008) is a hand-held condensation particle counter that can count the total number of particle within the size range of 0.01 to about 1 µm. The device was placed inside the styrofoam box for temperature insulation, with a 10 cm length of conductive tubing serving as an inlet, extending through the wall of the box to the outside. The CPC operates by continuously drawing aerosol samples in laminar flow through a heated saturator, followed by a cooled condenser where isopropyl alcohol vapor condenses onto the aerosol particles. As the resulting droplets grow to about 100 nm, they are counted by an optical detector. The growth rate of the particles is controlled by the temperature difference between the saturator and the condenser, which is regulated by the voltage applied to the thermoelectric device (TED). For this campaign, the TED was set to 2000 mV. To ensure consistent measurements, the isopropyl alcohol wick was re-soaked prior to each flight.

The CPC was calibrated prior to the campaign through comparison with a Scanning Mobility Particle Sizer (SMPS; model 3938, TSI Inc.) and a CPC (model 3776, TSI Inc.), following the procedures described by Hämeri et al. (2002) and Wiedensohler et al. (2018). The result is shown in Section S3 of the Supplement. The lower detection limit of the CPC, expressed as the cut-off diameter (D_{50}) at 50% counting efficiency, was measured to be 10.8 nm with an uncertainty of ± 0.076 nm (Table S1). The counting efficiency curve from the calibration is shown in Fig. S5. An intercomparison between the CPC in-flight measurements and the Differential Mobility Particle Sizer (DMPS) measurements (Backman et al., 2025) at the Sammaltunturi station at the same height within ±40 m is shown in Fig. S6. The results show strong agreement between the instruments, with a statistically significant correlation ($p < 0.05$, $R^2 = 0.97$), and a linear regression slope of 1.06.

The POPS (POPS, Handix Inc.) (Gao et al., 2016; Telg et al., 2017; Liu et al., 2021; Creamean et al., 2021; Pilz et al., 2022; Pohorsky et al., 2024b) is an optical particle spectrometer for measuring aerosol number concentrations and size distributions, and it is widely used on uncrewed airborne platforms. The POPS used in this study was a balloon-configured version of the instrument designed by the manufacturer, which has a foam enclosure (2.5 cm thick) with a pass-through for the sample inlet tubing. It was attached to the bottom of the setup. Aerosol particles are pulled through an inlet nozzle, after which they intersect a 405 nm diode laser beam. The scattered light is collected and focused onto a photomultiplier tube, which generates an electrical current proportional to the intensity of the scattered light. This intensity is influenced by the optical properties of the sampled particles, such as their size, shape, and refractive index.

For POPS, the optical response of particles was checked using reference polystyrene latex (PSL) spheres. The PSL equivalent diameter is defined as the diameter of an ideal, spherical, non-porous PSL particle that produces an optical signal equivalent to that of the particle being analysed. The POPS measures aerosol particles within the size range of 0.12–3.4 µm in 16 bins; how-

https://doi.org/10.5194/essd-2026-135
Preprint. Discussion started: 28 April 2026

ever, the effective upper limit for reliable detection is approximately 3 µm as reported by Pilz et al. (2022) and Pohorsky et al. (2024b). In addition, sizing uncertainties increase substantially in the first few bins. Therefore, the lowest and highest POPS size bins should be interpreted with caution. The POPS was calibrated by the manufacturer and used as such throughout the entire campaign. Our post-campaign in-house calibration results for POPS, including counting efficiency and PSL calibration, can be found in Sect. S4 of the Supplement.

Bezantakos and Biskos (2022) reported that operating temperatures can significantly affect CPC measurements. Additionally, the measured particle sizes and number concentrations may be affected by hygroscopic growth at high relative humidity. An experiment examining the temperature and relative humidity inside the payload under varying ambient conditions is presented in Section S5 of the Supplement. The results indicate that, following the initial warm-up period, the internal payload temperature stabilizes at more than 15 °C above the ambient temperature, while the relative humidity remains below 20%. Because the payload is always operating prior to launch, this experiment accurately represents the conditions under which the data were collected. The findings from this experiment are consistent with expectations, as the CPC and POPS were insulated, resulting in a stable and higher internal temperature than the ambient air temperature. As sampled air passed through the inlet tubing, it warmed up, leading to a reduction in its relative humidity compared to the surrounding air at the time of measurement. Consequently, the influence of outside air temperature on the condition inside this insulated payload is negligible, and the effect of hygroscopic growth is minimal. Similar findings were also found in other UAV-based studies (Nurowska et al., 2023; Julaha et al., 2025).

To further support this conclusion, an internal relative humidity parameter was estimated from in-flight measurements using the ambient temperature measured by the BME sensor and the internal temperature measured by the POPS. An example of the calculated in-flight relative humidity is shown in Fig. 4d, where the relative humidity remained below 50% even when the payload was in clouds. Across the full dataset, it was found that no data exceeded 80% RH, and most measurements were taken at relatively dry conditions (mostly below 60% RH). This further illustrate the minimal effect of hygroscopic growth on in-flight measurements. Furthermore, except on the final day of the campaign, the payload always operated below 3 km altitude, corresponding to the pressure range identified by Bezantakos and Biskos (2022) as having no effect on CPC measurements.

The mCDA (Palas GmbH) is a prototype mini cloud droplet analyzer, developed by Palas GmbH. It can measure cloud droplets ranging from 1 to 100 µm in 256 bins up to 500 particles per cubic meter. During this campaign, however, the first 81 bins were not utilized, leaving 175 active bins. The mCDA has dimensions of 160 x 110 x 290 mm, weighs 1.2 kg, and consumes less than 10 W of power. It was mounted on top of the styrofoam box with a 10 cm vertical inlet exposed to the environment, and the flow was maintained at 2.8 $\mathrm{L min^{-1}}$ with an air blower. The number size distribution of the sampled air was determined by the optical light scattering by individual particles. The mCDA was calibrated at FMI before and after the campaign using MonoDust 1500 calibration standard while adhering to the manufacturer's single size calibration procedure. The mCDA inlet was not dried; therefore, aerosol particles and cloud droplets were sampled simultaneously. To identify in-cloud periods, a cloud mask was used, defined by RH measurement of 100% and a total concentration of droplets larger than 2 µm exceeding 0.5 $\mathrm{cm^{-3}}$.

https://doi.org/10.5194/essd-2026-135
Preprint. Discussion started: 28 April 2026

Section S6 in the Supplement compares the mCDA with the full-sized Cloud Droplet Analyzer (CDA, Palas GMbH) (Doulgeris et al., 2025). The comparison were carried out at the station during PaCE2022 (Fig. S6) and during an intercomparison campaign (Doulgeris et al., 2026) organized by the ACTRIS RI Cloud In-Situ Topical Centre and conducted at the Sonnblick Observatory (3,106 m a.s.l) from 21th November to 3rd December 2022, immediately following PaCE2022 (Figs. S7-S8). These results indicate that even though discrepancies were found in the droplet number concentration, the effective radius agrees well between mCDA and CDA. This is consistent with the expectation that the cloud spectrometers provide robust droplet size measurements but derived parameters such as droplet number concentration and liquid water content are sensitive to inlet and sampling losses (e.g. Guyot et al. (2015); Doulgeris et al. (2020); Tiitta et al. (2022)). Thus, the mCDA cloud microphysics presented here should be interpreted with caution.

To further evaluate the performance of the payload directional stabilizer and the influence of inlet orientation and wind on aerosol measurements, total particle number concentrations from CPC, POPS, and mCDA were compared. In addition, particle number size distributions were examined at different stages of the flights. A detailed analysis and corresponding results are presented in Sect. S7. In brief, despite the horizontal inlet configuration of the CPC and POPS, their measurements are consistent with those obtained from the vertically oriented mCDA, indicating that the effects of inlet orientation and wind are minimal in this dataset.

For flights conducted between 16th and 28th September, the MPCK platforms was controlled by a gasoline winch. As a result, the emissions from the gasoline winch may influence POPS and CPC particle measurements. Data containing contaminated observations have been flagged by a `winch_contamination` flag, and a detailed discussion of the impact of gasoline emissions, as well as the method used to remove contaminated data, is provided in Sect. S8 of the Supplement. The section also demonstrates that at 100 m above ground level, the influence of emissions is negligible, as the balloon is already above the plume.

https://doi.org/10.5194/essd-2026-135
Preprint. Discussion started: 28 April 2026

Open Access Earth System Science Data Discussions

4 Dataset overview

Table 1. Overview of flights with the payload during PaCE campaign.

Date	Logbook note	Starting time (UTC)	Landing time (UTC)	Data availability
16/09/2022	Profiling and hovering, in-clouds	07:15	10:30	BME, CPC, POPS, mCDA
17/09/2022	Profiling and hovering, in-clouds	10:45	13:30	BME, CPC, POPS, mCDA
18/09/2022	Profiling and hovering, in-clouds	07:20	13:50	BME, CPC, POPS, mCDA
19/09/2022	Profiling and hovering, light drizzle	12:45	15:20	BME, CPC, POPS, mCDA
20/09/2022	Profiling and hovering, in-clouds	07:10	13:30	BME, CPC, POPS, mCDA
21/09/2022	Profiling and hovering	07:10	14:00	BME, CPC, POPS, mCDA
21/09/2022	Profiling, drizzle	16:45	19:45	BME, CPC, POPS, mCDA
22/09/2022	Staircase profiling, no clouds	09:00	15:45	BME, CPC, POPS, mCDA
23/09/2022	Profiling and hovering, in-clouds	06:45	09:00	BME, CPC, mCDA
23/09/2022	Profiling and hovering, in-clouds	16:00	19:45	BME, CPC, mCDA
27/09/2022	Staircase profiling, in-clouds	10:15	16:20	BME, CPC, mCDA
28/09/2022	Profiling and hovering, in-clouds	07:00	15:15	BME, CPC, mCDA
29/09/2022	Profiling and hovering, in-clouds	09:30	16:00	BME, CPC, mCDA
30/09/2022	Profiling and hovering, in-clouds	07:45	10:45	BME, CPC, mCDA
30/09/2022	Profiling and hovering, in-clouds	15:45	17:28	BME, CPC, mCDA
01/10/2022	Profiling and hovering, in-clouds	09:45	15:15	BME, CPC, POPS, mCDA
02/10/2022	Profiling and hovering, in-clouds	10:15	14:50	BME, CPC, POPS, mCDA
03/10/2022	Profiling and hovering, in-clouds	08:00	17:00	BME, CPC, POPS, mCDA
04/10/2022	Profiling and hovering, in-clouds	06:00	16:00	BME, CPC, POPS, mCDA
08/10/2022	Profiling, no clouds	13:50	16:00	BME, CPC, POPS, mCDA
10/10/2022	Profiling	08:00	12:30	BME, CPC, POPS, mCDA

The first flight carrying the FMI payload took place on 16th September, and the final flight on 10th October. In total, 21 flights were conducted, with more than one flight performed on some days. An overview of all flights is provided in Table 1.

For each flight, data from all the instruments was combined into a single file for release and further analysis. These files were given in ASCII comma-separated values (CSV) and NetCDF format. An overview description of csv files is shown in Table 2. The naming convention is FMI.TBS.b1.yyyyMMdd.hhmm.csv or FMI.TBS.b1.yyyyMMdd.hhmm.nc, where:

- FMI is the institute identifier (Finnish Meteorological Institute).
- TBS is the platform identifier (Tethered Balloon System)
- b1 is the data file processing level, with quality control applied. All data were carefully monitored and quality controlled. Missing or bad values were set to -9999.9.

https://doi.org/10.5194/essd-2026-135
Preprint. Discussion started: 28 April 2026

Open Access Earth System Science Data Discussions

Table 2. Data description of csv files.

Column name	Description	Instrument
datetime (utc)	Date and time of the data point from all the instruments in UTC	Raspberry pi
temp_bme (C)	Ambient temperature ($^{\circ}$C)	BME280
press_bme (hPa)	Ambient pressure (hPa)	
rh_bme (%)	Ambient relative humidity (%)	
height_bme (m)	Calculated height above ground level	
N_conc_cpc (cm-3)	Particle number concentration (cm^{-3})	CPC
press_cpc(hPa)	Inlet pressure (hPa)	
N_conc_pops (cm-3)	Particle number concentration (cm^{-3})	POPS
press_pops (hPa)	Inlet pressure (hPa)	
flow_rate_pops (cm3/s)	Inlet flow rate ($\mathrm{cm}^3\ \mathrm{s}^{-1}$)	
temp_pops (C)	POPS internal temperature	
rh_pops (%)	Calculated relative humidity inside POPS	
binX_pops (cm-3)	Aerosol number concentration (cm^{-3}) in binX, with X ranging from 1 to 16	
binX_pops (dN/dlogDp)	Normalized aerosol concentration (dN/dlogDp) in binX, with X ranging from 1 to 16	
binX_mcda (cm-3)	Number concentration (cm^{-3}) in binX, with X ranging from 1 to 175	mCDA
pm1_mcda	Particulate matters with diameter less than 1 micron (µg cm^{-3})	
pm25_mcda	Particulate matters with diameter less than 2.5 micron (µg cm^{-3})	
pm10_mcda	Particulate matters with diameter less than 10 micron (µg cm^{-3})	
binX_mcda (dN/dlogDp)	Normalized cloud droplet concentration (dN/dlogDp) in binX, with X ranging from 1 to 175	
Nd_mcda (cm-3)	Total cloud droplet concentration (cm^{-3})	
LWC_mcda (g/m3)	Liquid water content (g m^{-3})	
MVD_mcda (um)	Median volume diameter (µm)	
ED_mcda (um)	Effective droplet diameter (µm)	
winch_contamination	Flag indicating contamination from the winch	

- yyyyMMdd is the file date (UTC) in year, month and day format
- hhmm is the start time (UTC) in hours and minutes format
- csv or nc is the file format (Comma-Separated Values or NetCDF)

In all flights, the payload was recovered safely and remained under control, except on 10th October, when the balloon drifted freely. Additionally, the payload was continuously raised and lowered at a slow vertical velocity of 0.15-0.4 $\mathrm{m\,s}^{-1}$, resulting in minimal hysteresis effects.

For POPS, the normalized concentration (dN/dlogD_p) was derived in 16 PSL equivalent bins: 0.12 - 0.13 µm, 0.13 - 0.14 µm, 0.14 - 0.15 µm, 0.15 - 0.17 µm, 0.17 - 0.19 µm, 0.19 - 0.21 µm, 0.21 - 0.25 µm, 0.25 - 0.35 µm, 0.35 - 0.48 µm, 0.48 - 0.58 µm, 0.58 - 0.86 µm, 0.86 - 1.22 µm, 1.22 - 1.53 µm, 1.53 - 1.99 µm, 1.99 - 2.58 µm, 2.58 - 3.37 µm. The POPS internal

https://doi.org/10.5194/essd-2026-135
Preprint. Discussion started: 28 April 2026

relative humidity was derived based on the POPS internal temperature and ambient temperature and relative humidity obtained from BME.

From 16th of September to 2nd of October, the normalized concentration ($dN/dlogD_p$) was calculated from mCDA across 175 water-equivalent bins, with values ranging from 0.6 µm to 41.8 µm. On the 3rd of October, the mCDA was recalibrated, adjusting the 175 bins to span from 1.4 µm to 99.6 µm. The precise range of each size bin is provided in the data. Additionally, total cloud droplet number concentration (N_d), liquid water content (LWC), median droplet volume diameter (MVD), and effective droplet volume diameter (ED) were also derived based on the measured cloud droplet concentration, following Doulgeris et al. (2020). It should be noted that these parameters were only available when the payload was in the cloud. This condition was identified using a cloud mask, defined by an ambient relative humidity of 100% and a total concentration of droplets larger than 2 µm exceeding 0.5 cm^{-3}.

The RH measurements from BME occasionally remained saturated at 100% after exiting a cloud, likely due to condensation forming on the sensor. To mitigate this issue, RH data was filtered out when the RH remained at 100% but the cloud mask criteria were not satisfied.

On the 23rd of September, the internal pump inside the POPS experienced a failure, resulting in erroneous data from the 23rd to the 30th of September. This issue was eventually identified and resolved, allowing POPS data to be available again starting from 1th October. Except for this period, data collected from all the instruments are available simultaneously during all flights. An example of these harmonized data is shown in Fig. 4. In general, the duration for each flight was determined based on the weather conditions, such as cloud cover and wind speed. This guarantees both the safety of the operation and the scientific value of the data.

Figure 5 presents the meteorological conditions recorded by the payload across all the flights. The measured pressure ranged from 380 hPa to 1000 hPa, with the median pressure at around 900 hPa. The measured temperature varied from -22 to 23 °C with the median temperature at approximately 1 °C. The relative humidity spanned from 25 % to 100 %. Figure 6 illustrates LWC, MVD, ED, and normalized size distribution ($dN/dlogD_p$) derived from mCDA measurements across all the flights. A total of 19.34 hours of in-cloud measurements and 83.15 hours of no-cloud measurements were recorded. The median, 25th and 75th percentile of MVD was 9.5, 7.5, 12.0µm, and of ED was 8.4, 6.6, 10.3 µm. Figure 7 shows the measured total number concentration from CPC, POPS and mCDA across all the flights. Each instrument has a different cut-off diameter range: 0.01 - 1 µm for CPC, 0.12 - 3.4 µm for POPS (PSL equivalent), and 0.6 - 41.8 µm and 1.4 - 99.6 µm for mCDA (water equivalent). These differing size ranges result in differences in the measured number concentrations. In the whole campaign, when the payload was not in clouds, the median, 25th and 75th percentile of total number concentration from CPC was 314, 144, 650cm^{-3}, and from POPS was 35.5, 9.9, 80.1 cm^{-3}. Conversely, when the payload was in clouds, the median, 25th and 75th percentile of total number concentration from CPC was 206.5, 117, 300 cm^{-3}, from POPS was 36, 14, 67.2 cm^{-3} and of total N_d from mCDA was 8.8, 3.4, 18 cm^{-3} .

https://doi.org/10.5194/essd-2026-135
Preprint. Discussion started: 28 April 2026

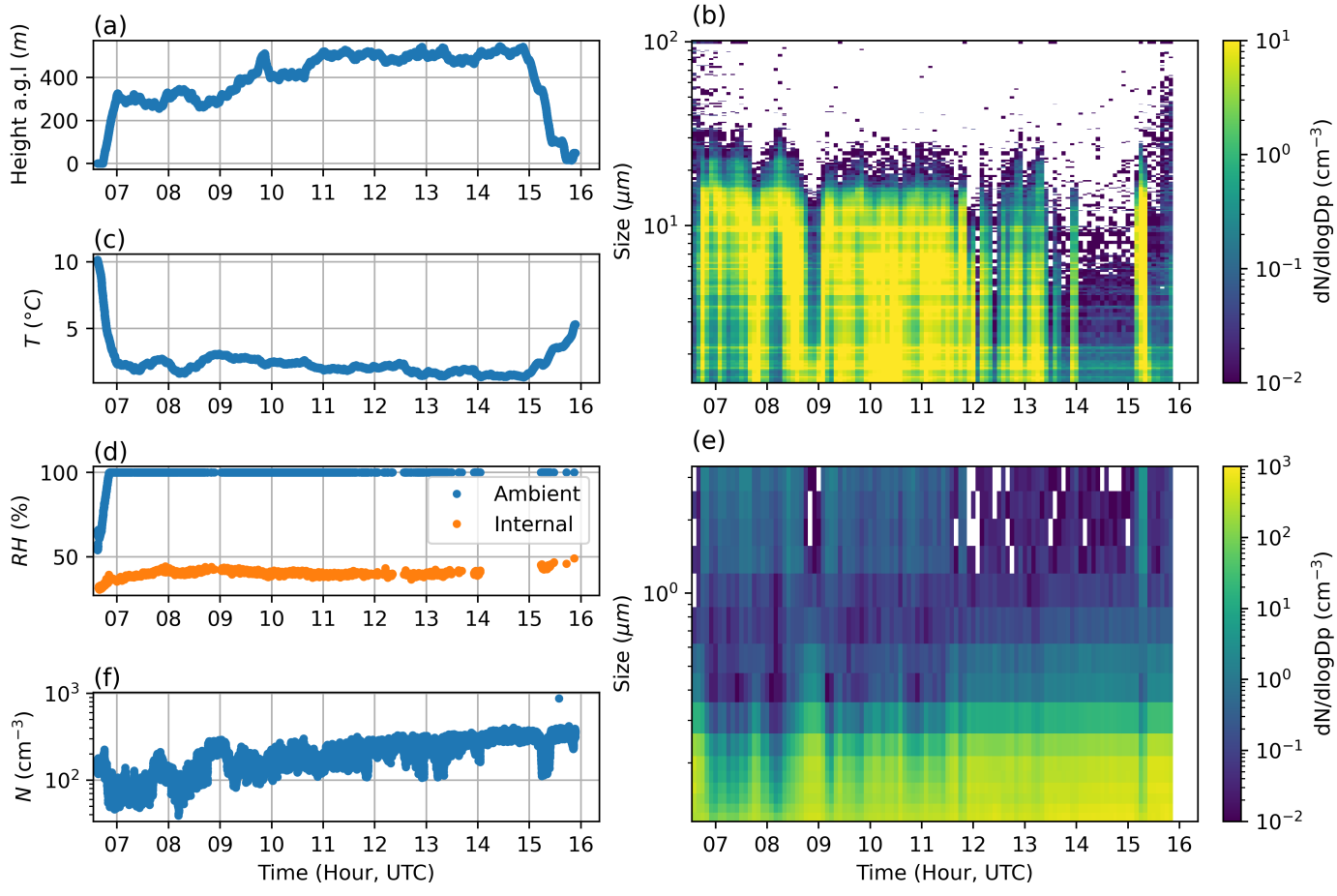

Figure 4. Measurements on the 4th of October flight from the FMI's payload. a) Height above ground level (m), b) dN/dlogD$_p$ (cm^{-3}) calculated from mCDA measurements, c) Temperature (°C) measured by BME280, d) Ambient relative humidity (%) measured by BME280 and calculated internal relative humidity, e) dN/dlogD$_p$ (cm^{-3}) calculated from POPS measurements and f) Number concentration (cm^{-3}) from CPC. Subplots (b) and (e) are averaged over 5 minutes for visualization.

https://doi.org/10.5194/essd-2026-135
Preprint. Discussion started: 28 April 2026

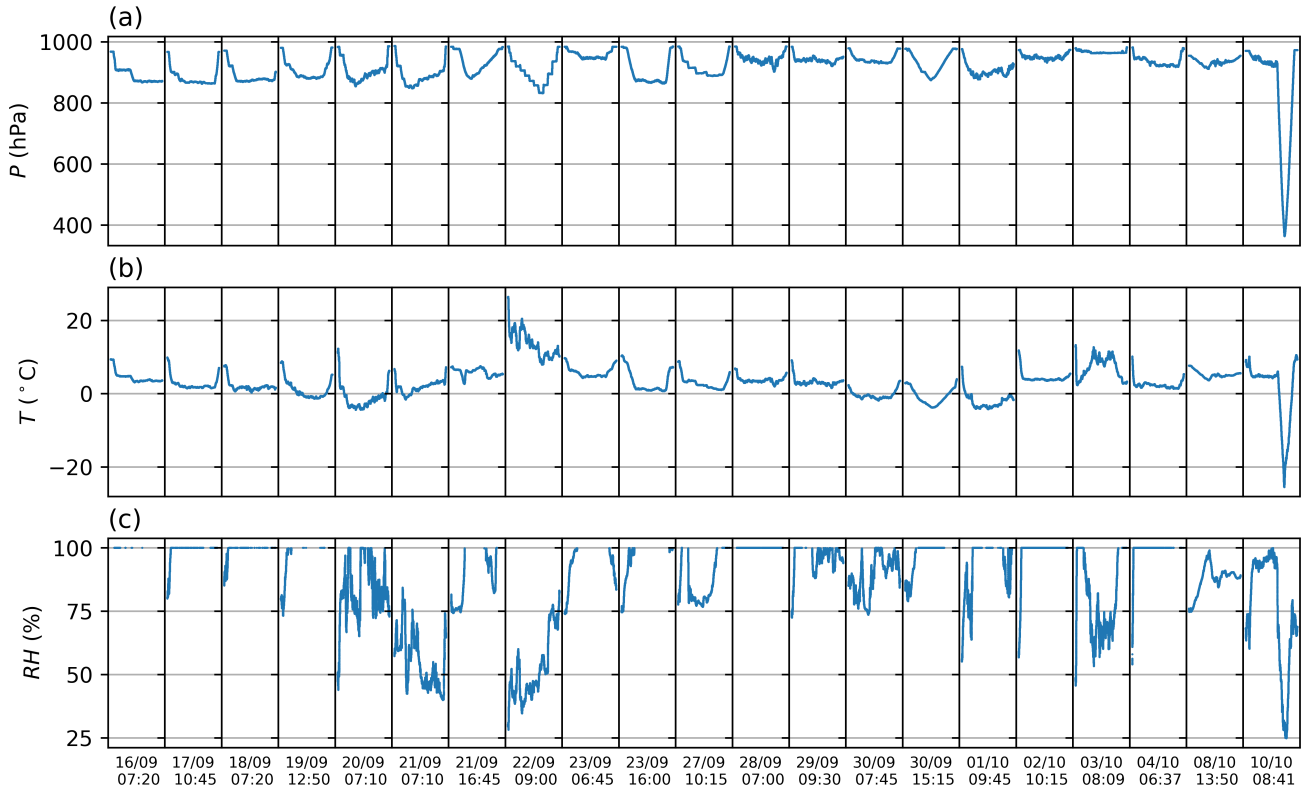

Figure 5. Overview of meteorological parameters measured by the FMI's payload: a) Pressure (hPa), b) Temperature (°C) and c) Relative humidity (RH) measured by BME280. The x-axis shows the flight starting time in UTC.

https://doi.org/10.5194/essd-2026-135
Preprint. Discussion started: 28 April 2026

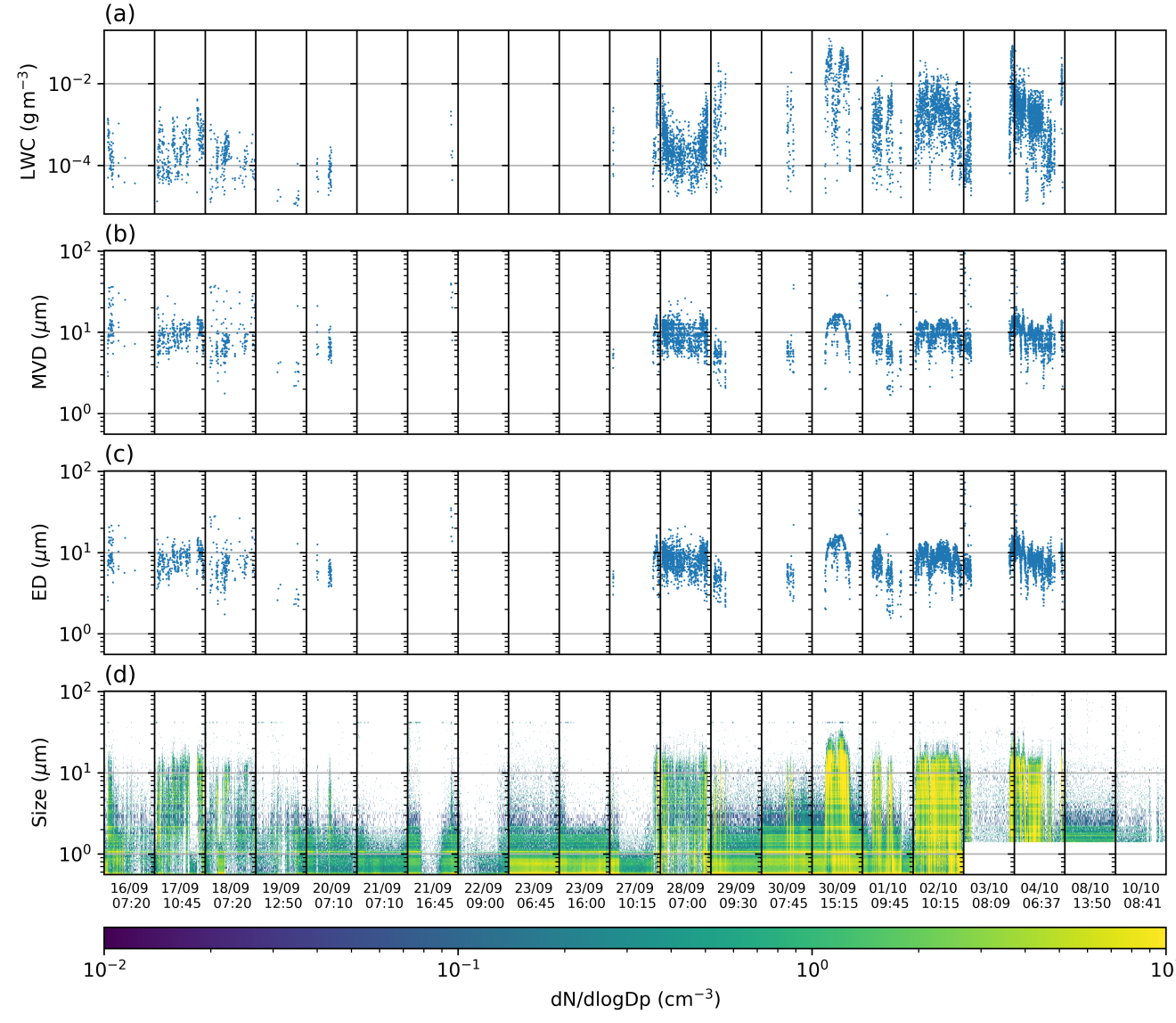

Figure 6. Overview of a) Liquid water content (g m^{-3}), b) Median volume diameter (μm), c) Effective diameter (μm), and d) dN/dlogD_p (cm^{-3}) calculated from mCDA measurements from all the flights. The x-axis shows the flight starting time in UTC.

https://doi.org/10.5194/essd-2026-135
Preprint. Discussion started: 28 April 2026

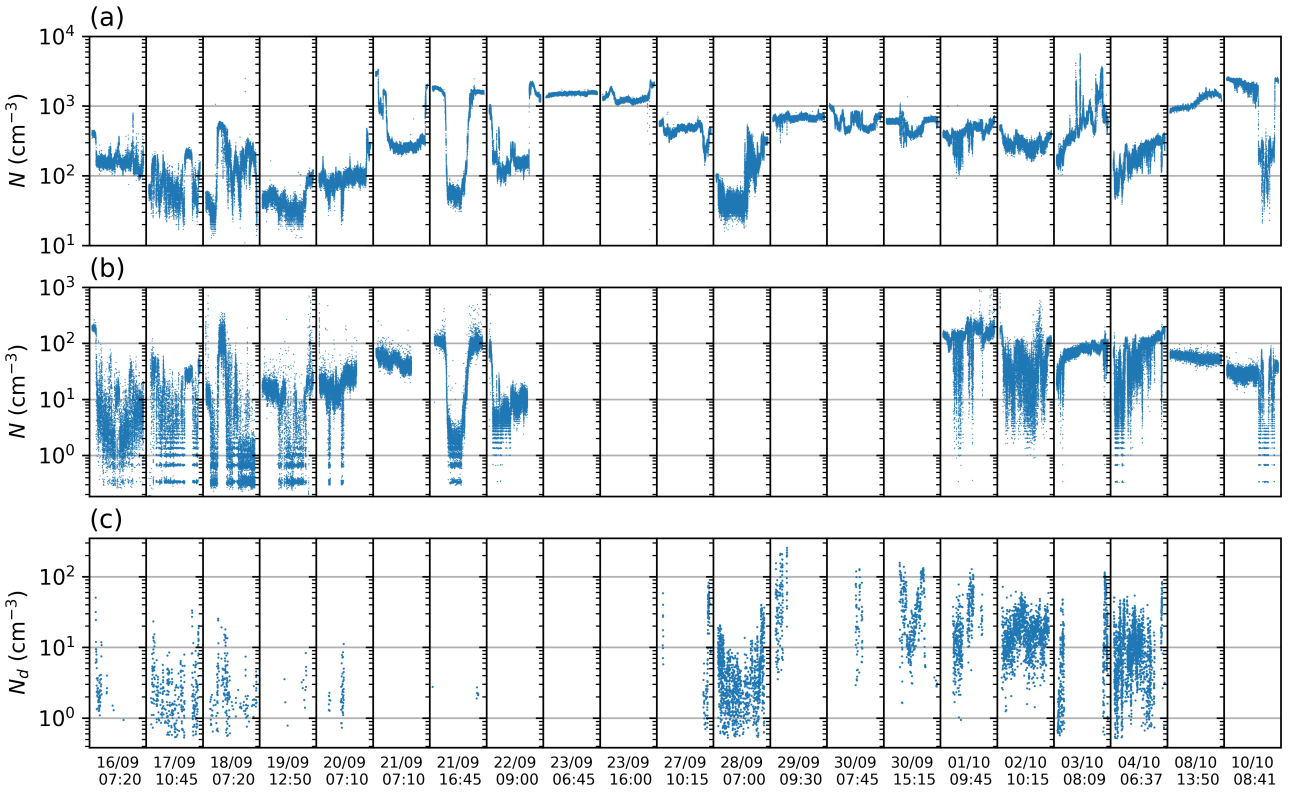

Figure 7. Overview of number concentration (cm^{-3}) from a) CPC b) POPS, and c) mCDA from all the flights. Only data unaffected by the winch The x-axis shows the flight starting time in UTC.

https://doi.org/10.5194/essd-2026-135
Preprint. Discussion started: 28 April 2026

5 Summary

This paper provides an overview of the data collected during the PaCE 2022 campaign in Pallas, Finnish sub-Arctic, from September to December 2022, representing the first deployment of an FMI payload on tethered balloon systems. In Section 2, we provided an overview of the campaign as well as the deployed TBS. In Section 3, we described the payload instrument setup, the associated measurement uncertainty, and the validation against reference instruments. Section 4 presented a description of the dataset, its processing procedure, and an overview of the measured parameters.

This dataset is part of the data collected during the PaCE 2022 campaign. In addition, other platforms such as uncrewed aerial vehicles, ground-based in-situ instruments, and ground-based remote sensing instruments were deployed concurrently. Together, this diverse dataset provides a comprehensive set of observations of atmospheric properties across various research topics. For instance, the cloud measurements from the TBSs can be used to validate cloud microphysical properties derived from lidars and cloud radars, as outlined by (Frisch et al., 2002; Donovan et al., 2015; Vivekanandan et al., 2020).

https://doi.org/10.5194/essd-2026-135
Preprint. Discussion started: 28 April 2026

Open Access Earth System Science Data Discussions

6 Data availability

This dataset (Le et al., 2026) is available at https://doi.org/10.5281/zenodo.18432043, last access 17 February 2026. It was published at the Zenodo Open Science data archive, under a dedicated community Pallas Cloud Experiment – PaCE2022.

Author contributions. DB and KD planned and coordinated the FMI flights during PaCE 2022 campaign. All authors conducted the airborne measurements. VL and DB processed, analyzed, and quality-controlled FMI dataset. DB designed the payload. VL prepared the manuscript and all authors contributed to manuscript editing.

Competing interests. At least one of the (co-)authors serves as topic editor for the special issue to which this paper belongs.

Acknowledgements. The authors would like to express their gratitude to the Metsähallitus personnel, especially Mirka Hatanpää, for their invaluable support during the Pallas Cloud Experiment 2022.

Financial support. This work was supported ACTRIS-Finland funding through the Ministry of Transport and Communications, the Atmosphere and Climate Competence Center Flagship funding by the Research Council of Finland (Grants 337552). This project has also received funding from the European Union, H2020 research and innovation program (ACTRIS-IMP, the European Research Infrastructure for the observation of Aerosol, Clouds, and Trace gases, Grant 871115). Financial support from the Magnus Ehrnrooth foundation is greatly appreciated. This work was also supported by the Research Council of Finland - project 4Dcloud (decision 369600).

https://doi.org/10.5194/essd-2026-135
Preprint. Discussion started: 28 April 2026

References

Abbatt, J. P. D., Leaitch, W. R., Aliabadi, A. A., Bertram, A. K., Blanchet, J.-P., Boivin-Rioux, A., Bozem, H., Burkart, J., Chang, R. Y. W., Charette, J., Chaubey, J. P., Christensen, R. J., Cirisan, A., Collins, D. B., Croft, B., Dionne, J., Evans, G. J., Fletcher, C. G., Galí, M., Ghahreman, R., Girard, E., Gong, W., Gosselin, M., Gourdal, M., Hanna, S. J., Hayashida, H., Herber, A. B., Hesaraki, S., Hoor, P., Huang, L., Hussherr, R., Irish, V. E., Keita, S. A., Kodros, J. K., Köllner, F., Kolonjari, F., Kunkel, D., Ladino, L. A., Law, K., Levasseur, M., Libois, Q., Liggio, J., Lizotte, M., Macdonald, K. M., Mahmood, R., Martin, R. V., Mason, R. H., Miller, L. A., Moravek, A., Mortenson, E., Mungall, E. L., Murphy, J. G., Namazi, M., Norman, A.-L., O'Neill, N. T., Pierce, J. R., Russell, L. M., Schneider, J., Schulz, H., Sharma, S., Si, M., Staebler, R. M., Steiner, N. S., Thomas, J. L., von Salzen, K., Wentzell, J. J. B., Willis, M. D., Wentworth, G. R., Xu, J.-W., and Yakobi-Hancock, J. D.: Overview paper: New insights into aerosol and climate in the Arctic, Atmospheric Chemistry and Physics, 19, 2527–2560, https://doi.org/10.5194/acp-19-2527-2019, 2019.

Aitken, J.: Dust, Fogs, and Clouds, Nature, 23, 384–385, https://doi.org/10.1038/023384a0, 1881.

Ancellet, G., Pelon, J., Blanchard, Y., Quennehen, B., Bazureau, A., Law, K. S., and Schwarzenboeck, A.: Transport of aerosol to the Arctic: analysis of CALIOP and French aircraft data during the spring 2008 POLARCAT campaign, Atmospheric Chemistry and Physics, 14, 8235–8254, https://doi.org/10.5194/acp-14-8235-2014, 2014.

Backman, J., Luoma, K., Servomaa, H., Vakkari, V., and Brus, D.: In-situ aerosol measurements at the Arctic Sammaltunturi measurement station during the Pallas Cloud Experiment 2022, Earth System Science Data Discussions, pp. 1–22, https://doi.org/10.5194/essd-2025-284, 2025.

Barbieri, L., Kral, S. T., Bailey, S. C. C., Frazier, A. E., Jacob, J. D., Reuder, J., Brus, D., Chilson, P. B., Crick, C., Detweiler, C., Doddi, A., Elston, J., Foroutan, H., González-Rocha, J., Greene, B. R., Guzman, M. I., Houston, A. L., Islam, A., Kemppinen, O., Lawrence, D., Pillar-Little, E. A., Ross, S. D., Sama, M. P., Schmale, D. G., Schuyler, T. J., Shankar, A., Smith, S. W., Waugh, S., Dixon, C., Borenstein, S., and de Boer, G.: Intercomparison of Small Unmanned Aircraft System (sUAS) Measurements for Atmospheric Science during the LAPSE-RATE Campaign, Sensors, 19, https://doi.org/10.3390/s19092179, 2019.

Bekryaev, R. V., Polyakov, I. V., and Alexeev, V. A.: Role of Polar Amplification in Long-Term Surface Air Temperature Variations and Modern Arctic Warming, Journal of Climate, 23, 3888 – 3906, https://doi.org/10.1175/2010JCLI3297.1, 2010.

Bezantakos, S. and Biskos, G.: Temperature and pressure effects on the performance of the portable TSI 3007 condensation particle counter: Implications on ground and aerial observations, Journal of Aerosol Science, 159, 105 877, https://doi.org/10.1016/j.jaerosci.2021.105877, 2022.

Borys, R. D.: Studies of ice nucleation by Arctic aerosol on AGASP-II, Journal of Atmospheric Chemistry, 9, 169–185, https://doi.org/10.1007/BF00052831, 1989.

Browell, E. V., Butler, C. F., Kooi, S. A., Fenn, M. A., Harriss, R. C., and Gregory, G. L.: Large-scale variability of ozone and aerosols in the summertime Arctic and sub-Arctic troposphere, Journal of Geophysical Research: Atmospheres, 97, 16 433–16 450, https://doi.org/10.1029/92JD00159, _eprint: https://agupubs.onlinelibrary.wiley.com/doi/pdf/10.1029/92JD00159, 1992.

Brus, D., Gustafsson, J., Vakkari, V., Kemppinen, O., de Boer, G., and Hirsikko, A.: Measurement report: Properties of aerosol and gases in the vertical profile during the LAPSE-RATE campaign, Atmospheric Chemistry and Physics, 21, 517–533, https://doi.org/10.5194/acp-21-517-2021, 2021.

Cao, Y., Liang, S., Chen, X., He, T., Wang, D., and Cheng, X.: Enhanced wintertime greenhouse effect reinforcing Arctic amplification and initial sea-ice melting, Scientific Reports, 7, 8462, https://doi.org/10.1038/s41598-017-08545-2, 2017.

https://doi.org/10.5194/essd-2026-135
Preprint. Discussion started: 28 April 2026

Chávez-Medina, V., Khodamoradi, H., Schlenczek, O., Nordsiek, F., Brunner, C. E., Bodenschatz, E., and Bagheri, G.: Max Planck WinDarts: High-Resolution Atmospheric Boundary Layer Measurements with the Max Planck CloudKite platform and Ground Weather Station – A Data Overview, Earth System Science Data Discussions, 2025, 1–22, https://doi.org/10.5194/essd-2025-111, 2025.

Creamean, J. M., de Boer, G., Telg, H., Mei, F., Dexheimer, D., Shupe, M. D., Solomon, A., and McComiskey, A.: Assessing the vertical structure of Arctic aerosols using balloon-borne measurements, Atmospheric Chemistry and Physics, 21, 1737–1757, https://doi.org/10.5194/acp-21-1737-2021, 2021.

Curry, J. A., Ebert, E. E., and Herman, G. F.: Mean and turbulence structure of the summertime Arctic cloudy boundary layer, Quarterly Journal of the Royal Meteorological Society, 114, 715–746, https://doi.org/10.1002/qj.49711448109, 1988.

Dada, L., Angot, H., Beck, I., Baccarini, A., Quéléver, L. L. J., Boyer, M., Laurila, T., Brasseur, Z., Jozef, G., de Boer, G., Shupe, M. D., Henning, S., Bucci, S., Dütsch, M., Stohl, A., Petäjä, T., Daellenbach, K. R., Jokinen, T., and Schmale, J.: A central arctic extreme aerosol event triggered by a warm air-mass intrusion, Nature Communications, 13, 5290, https://doi.org/10.1038/s41467-022-32872-2, 2022.

Davy, R. and Outten, S.: The Arctic Surface Climate in CMIP6: Status and Developments since CMIP5, Journal of Climate, 33, 8047 – 8068, https://doi.org/10.1175/JCLI-D-19-0990.1, place: Boston MA, USA, 2020.

Donovan, D. P., Klein Baltink, H., Henzing, J. S., De Roode, S. R., and Siebesma, A. P.: A depolarisation lidar-based method for the determination of liquid-cloud microphysical properties, Atmospheric Measurement Techniques, 8, 237–266, https://doi.org/10.5194/amt-8-237-2015, 2015.

Doulgeris, K.-M., Komppula, M., Romakkaniemi, S., Hyvärinen, A.-P., Kerminen, V.-M., and Brus, D.: In situ cloud ground-based measurements in the Finnish sub-Arctic: intercomparison of three cloud spectrometer setups, Atmospheric Measurement Techniques, 13, 5129–5147, https://doi.org/10.5194/amt-13-5129-2020, 2020.

Doulgeris, K. M., Lihavainen, H., Hyvärinen, A.-P., Kerminen, V.-M., and Brus, D.: An extensive data set for in situ microphysical characterization of low-level clouds in a Finnish sub-Arctic site, Earth System Science Data, 14, 637–649, https://doi.org/10.5194/essd-14-637-2022, 2022.

Doulgeris, K. M., Vakkari, V., O'Connor, E. J., Kerminen, V.-M., Lihavainen, H., and Brus, D.: Influence of air mass origin on microphysical properties of low-level clouds in a subarctic environment, Atmospheric Chemistry and Physics, 23, 2483–2498, https://doi.org/10.5194/acp-23-2483-2023, 2023.

Doulgeris, K. M., Kaikkonen, V., Juttula, H., Molkoselkä, E., Mäkynen, A., and Brus, D.: In situ surface cloud measurement dataset from four cloud spectrometers during the Pallas Cloud Experiment (PaCE) 2022, Earth System Science Data, 17, 6497–6506, https://doi.org/10.5194/essd-17-6497-2025, 2025.

Doulgeris, K. M., et al, and et al: Evaluation of cloud spectrometers and one holographic imaging probe during the Aerosol, Clouds and Trace Gases Research Infrastructure (ACTRIS) cloud in situ intercomparison campaign under sub-zero conditions at Sonnblick Observatory., submitted to Atmos. Meas. Tech, 2026.

Esau, I., Pettersson, L. H., Cancet, M., Chapron, B., Chernokulsky, A., Donlon, C., Sizov, O., Soromotin, A., and Johannesen, J. A.: The Arctic Amplification and Its Impact: A Synthesis through Satellite Observations, Remote Sensing, 15, https://doi.org/10.3390/rs15051354, 2023.

Ferrero, L., Ritter, C., Cappelletti, D., Moroni, B., Močnik, G., Mazzola, M., Lupi, A., Becagli, S., Traversi, R., Cataldi, M., Neuber, R., Vitale, V., and Bolzacchini, E.: Aerosol optical properties in the Arctic: The role of aerosol chemistry and dust composition in a closure experiment between Lidar and tethered balloon vertical profiles, Science of The Total Environment, 686, 452–467, https://doi.org/10.1016/j.scitotenv.2019.05.399, 2019.

https://doi.org/10.5194/essd-2026-135
Preprint. Discussion started: 28 April 2026

Forster, P., Storelvmo, T., Armour, K., Collins, W., Dufresne, J.-L., Frame, D., Lunt, D. J., Mauritsen, T., Palmer, M. D., Watanabe, M., Wild, M., and Zhang, H.: The Earth's Energy Budget, Climate Feedbacks, and Climate Sensitivity, in: Climate Change 2021: The Physical Science Basis, Contribution of Working Group I to the Sixth Assessment Report of the Intergovernmental Panel on Climate Change, edited by Masson-Delmotte, V., Zhai, P., Pirani, A., Connors, S. L., Péan, C., Berger, S., Caud, N., Chen, Y., Goldfarb, L., Gomis, M. I., Huang, M., Leitzell, K., Lonnoy, E., Matthews, J. B. R., Maycock, T. K., Waterfield, T., Yelekçi, O., Yu, R., and Zhou, B., pp. 923–1054, Cambridge University Press, Cambridge, UK and New York, NY, USA, https://doi.org/10.1017/9781009157896.009, 2021.

Frisch, S., Shupe, M., Djalalova, I., Feingold, G., and Poellot, M.: The Retrieval of Stratus Cloud Droplet Effective Radius with Cloud Radars, Journal of Atmospheric and Oceanic Technology, 19, 835 – 842, https://doi.org/10.1175/1520-0426(2002)019<0835:TROSCD>2.0.CO;2, 2002.

Gao, R. S., Telg, H., McLaughlin, R. J., Ciciora, S. J., Watts, L. A., Richardson, M. S., Schwarz, J. P., Perring, A. E., Thornberry, T. D., Rollins, A. W., Markovic, M. Z., Bates, T. S., Johnson, J. E., and Fahey, D. W.: A light-weight, high-sensitivity particle spectrometer for PM2.5 aerosol measurements, Aerosol Science and Technology, 50, 88–99, https://doi.org/10.1080/02786826.2015.1131809, 2016.

Guyot, G., Gourbeyre, C., Febvre, G., Shcherbakov, V., Burnet, F., Dupont, J.-C., Sellegri, K., and Jourdan, O.: Quantitative evaluation of seven optical sensors for cloud microphysical measurements at the Puy-de-Dôme Observatory, France, Atmospheric Measurement Techniques, 8, 4347–4367, https://doi.org/10.5194/amt-8-4347-2015, 2015.

Hara, K., Osada, K., and Yamanouchi, T.: Tethered balloon-borne aerosol measurements: seasonal and vertical variations of aerosol constituents over Syowa Station, Antarctica, Atmospheric Chemistry and Physics, 13, 9119–9139, https://doi.org/10.5194/acp-13-9119-2013, 2013.

Holland, M. M. and Bitz, C. M.: Polar amplification of climate change in coupled models, Climate Dynamics, 21, 221–232, https://doi.org/10.1007/s00382-003-0332-6, 2003.

Huang, Y., Dong, X., Kay, J. E., Xi, B., and McIlhattan, E. A.: The climate response to increased cloud liquid water over the Arctic in CESM1: a sensitivity study of Wegener–Bergeron–Findeisen process, Climate Dynamics, 56, 3373–3394, https://doi.org/10.1007/s00382-021-05648-5, 2021.

Hämeri, K., Koponen, I. K., Aalto, P. P., and Kulmala, M.: The particle detection efficiency of the TSI-3007 condensation particle counter, Journal of Aerosol Science, 33, 1463–1469, https://doi.org/10.1016/S0021-8502(02)00090-3, 2002.

Julaha, K., Ždímal, V., Mbengue, S., Brus, D., and Zíková, N.: Drone-based vertical profiling of particulate matter size distribution and carbonaceous aerosols: urban vs. rural environment, Atmospheric Chemistry and Physics, 25, 17 933–17 951, https://doi.org/10.5194/acp-25-17933-2025, 2025.

Kay, J. E. and Gettelman, A.: Cloud influence on and response to seasonal Arctic sea ice loss, Journal of Geophysical Research: Atmospheres, 114, https://doi.org/10.1029/2009JD011773, 2009.

Kay, J. E., L'Ecuyer, T., Chepfer, H., Loeb, N., Morrison, A., and Cesana, G.: Recent Advances in Arctic Cloud and Climate Research, Current Climate Change Reports, 2, 159–169, https://doi.org/10.1007/s40641-016-0051-9, 2016.

Komppula, M., Lihavainen, H., Kerminen, V.-M., Kulmala, M., and Viisanen, Y.: Measurements of cloud droplet activation of aerosol particles at a clean subarctic background site, Journal of Geophysical Research: Atmospheres, 110, https://doi.org/10.1029/2004JD005200, 2005.

Lathem, T. L., Beyersdorf, A. J., Thornhill, K. L., Winstead, E. L., Cubison, M. J., Hecobian, A., Jimenez, J. L., Weber, R. J., Anderson, B. E., and Nenes, A.: Analysis of CCN activity of Arctic aerosol and Canadian biomass burning during summer 2008, Atmospheric Chemistry and Physics, 13, 2735–2756, https://doi.org/10.5194/acp-13-2735-2013, 2013.

https://doi.org/10.5194/essd-2026-135
Preprint. Discussion started: 28 April 2026

Le, V., Brus, D., Doulgeris, K., Komppula, M., Backman, J., Bagheri, G., and Bodenschatz, E.: Dataset of airborne measurements of aerosol, cloud droplets and meteorology by tethered balloon during PaCE 2022, Zenodo [data set], https://doi.org/10.5281/zenodo.18432043, 2026.

Lihavainen, H., Kerminen, V.-M., and Remer, L. A.: Aerosol-cloud interaction determined by both in situ and satellite data over a northern high-latitude site, Atmospheric Chemistry and Physics, 10, 10 987–10 995, https://doi.org/10.5194/acp-10-10987-2010, 2010.

Liu, Z., Osborne, M., Anderson, K., Shutler, J. D., Wilson, A., Langridge, J., Yim, S. H. L., Coe, H., Babu, S., Satheesh, S. K., Zuidema, P., Huang, T., Cheng, J. C. H., and Haywood, J.: Characterizing the performance of a POPS miniaturized optical particle counter when operated on a quadcopter drone, Atmospheric Measurement Techniques, 14, 6101–6118, https://doi.org/10.5194/amt-14-6101-2021, 2021.

Manabe, S. and Wetherald, R. T.: The Effects of Doubling the CO2 Concentration on the climate of a General Circulation Model, Journal of Atmospheric Sciences, 32, 3 – 15, https://doi.org/10.1175/1520-0469(1975)032<0003:TEODTC>2.0.CO;2, 1975.

Mordas, G., Manninen, H. E., Petäjä, T., Aalto, P. P., Hämeri, K., and Kulmala, M.: On Operation of the Ultra-Fine Water-Based CPC TSI 3786 and Comparison with Other TSI Models (TSI 3776, TSI 3772, TSI 3025, TSI 3010, TSI 3007), Aerosol Science and Technology, 42, 152–158, https://doi.org/10.1080/02786820701846252, 2008.

Nurowska, K., Mohammadi, M., Malinowski, S., and Markowicz, K.: Applicability of the low-cost OPC-N3 optical particle counter for microphysical measurements of fog, Atmospheric Measurement Techniques, 16, 2415–2430, https://doi.org/10.5194/amt-16-2415-2023, 2023.

Ono, J., Watanabe, M., Komuro, Y., Tatebe, H., and Abe, M.: Enhanced Arctic warming amplification revealed in a low-emission scenario, Communications Earth & Environment, 3, 27, https://doi.org/10.1038/s43247-022-00354-4, 2022.

Park, H.-S., Kim, S.-J., Stewart, A. L., Son, S.-W., and Seo, K.-H.: Mid-Holocene Northern Hemisphere warming driven by Arctic amplification, Science Advances, 5, eaax8203, https://doi.org/10.1126/sciadv.aax8203, 2019.

Philipp, D., Stengel, M., and Ahrens, B.: Analyzing the Arctic Feedback Mechanism between Sea Ice and Low-Level Clouds Using 34 Years of Satellite Observations, Journal of Climate, 33, 7479 – 7501, https://doi.org/10.1175/JCLI-D-19-0895.1, place: Boston MA, USA, 2020.

Pilz, C., Düsing, S., Wehner, B., Müller, T., Siebert, H., Voigtländer, J., and Lonardi, M.: CAMP: an instrumented platform for balloon-borne aerosol particle studies in the lower atmosphere, Atmospheric Measurement Techniques, 15, 6889–6905, https://doi.org/10.5194/amt-15-6889-2022, 2022.

Pohorsky, R., Baccarini, A., Brett, N., Barret, B., Bekki, S., Pappaccogli, G., Dieudonné, E., Temime-Roussel, B., D'Anna, B., Cesler-Maloney, M., Donateo, A., Decesari, S., Law, K. S., Simpson, W. R., Fochesatto, J., Arnold, S. R., and Schmale, J.: In situ vertical observations of the layered structure of air pollution in a continental high latitude urban boundary layer during winter, EGUsphere, 2024, 1–54, https://doi.org/10.5194/egusphere-2024-2863, 2024a.

Pohorsky, R., Baccarini, A., Tolu, J., Winkel, L. H. E., and Schmale, J.: Modular Multiplatform Compatible Air Measurement System (MoMuCAMS): a new modular platform for boundary layer aerosol and trace gas vertical measurements in extreme environments, Atmospheric Measurement Techniques, 17, 731–754, https://doi.org/10.5194/amt-17-731-2024, 2024b.

Rantanen, M., Karpechko, A. Y., Lipponen, A., Nordling, K., Hyvärinen, O., Ruosteenoja, K., Vihma, T., and Laaksonen, A.: The Arctic has warmed nearly four times faster than the globe since 1979, Communications Earth & Environment, 3, 168, https://doi.org/10.1038/s43247-022-00498-3, 2022.

Schlenczek, O., Nordsiek, F., Brunner, C. E., Chávez-Medina, V., Thiede, B., Bodenschatz, E., and Bagheri, G.: Airborne measurements of turbulence and cloud microphysics during PaCE 2022 using the Advanced Max Planck CloudKite Instrument (MPCK), Earth System Science Data Discussions, 2025, 1–29, https://doi.org/10.5194/essd-2025-112, 2025.

https://doi.org/10.5194/essd-2026-135
Preprint. Discussion started: 28 April 2026

Tan, I. and Storelvmo, T.: Evidence of Strong Contributions From Mixed-Phase Clouds to Arctic Climate Change, Geophysical Research Letters, 46, 2894–2902, https://doi.org/10.1029/2018GL081871, 2019.

Taylor, P. C., Cai, M., Hu, A., Meehl, J., Washington, W., and Zhang, G. J.: A Decomposition of Feedback Contributions to Polar Warming Amplification, Journal of Climate, 26, 7023 – 7043, https://doi.org/10.1175/JCLI-D-12-00696.1, 2013.

Telg, H., Murphy, D. M., Bates, T. S., Johnson, J. E., Quinn, P. K., Giardi, F., and Gao, R.-S.: A practical set of miniaturized instruments for vertical profiling of aerosol physical properties, Aerosol Science and Technology, 51, 715–723, https://doi.org/10.1080/02786826.2017.1296103, _eprint: https://doi.org/10.1080/02786826.2017.1296103, 2017.

Tiitta, P., Leskinen, A., Kaikkonen, V. A., Molkoselkä, E. O., Mäkynen, A. J., Joutsensaari, J., Calderon, S., Romakkaniemi, S., and Komppula, M.: Intercomparison of holographic imaging and single-particle forward light scattering in situ measurements of liquid clouds in changing atmospheric conditions, Atmospheric Measurement Techniques, 15, 2993–3009, https://doi.org/10.5194/amt-15-2993-2022, 2022.

Twomey, S.: The nuclei of natural cloud formation part II: The supersaturation in natural clouds and the variation of cloud droplet concentration, Geofisica pura e applicata, 43, 243–249, https://doi.org/10.1007/BF01993560, 1959.

Vavrus, S.: The Impact of Cloud Feedbacks on Arctic Climate under Greenhouse Forcing, Journal of Climate, 17, 603 – 615, https://doi.org/10.1175/1520-0442(2004)017<0603:TIOCFO>2.0.CO;2, 2004.

Vavrus, S., Waliser, D., Schweiger, A., and Francis, J.: Simulations of 20th and 21st century Arctic cloud amount in the global climate models assessed in the IPCC AR4, Climate Dynamics, 33, 1099–1115, https://doi.org/10.1007/s00382-008-0475-6, 2009.

Vivekanandan, J., Ghate, V. P., Jensen, J. B., Ellis, S. M., and Schwartz, M. C.: A Technique for Estimating Liquid Droplet Diameter and Liquid Water Content in Stratocumulus Clouds Using Radar and Lidar Measurements, Journal of Atmospheric and Oceanic Technology, 37, 2145 – 2161, https://doi.org/10.1175/JTECH-D-19-0092.1, 2020.

Wiedensohler, A., Wiesner, A., Weinhold, K., Birmili, W., Hermann, M., Merkel, M., Müller, T., Pfeifer, S., Schmidt, A., Tuch, T., Velarde, F., Quincey, P., Seeger, S., and Nowak, A.: Mobility particle size spectrometers: Calibration procedures and measurement uncertainties, Aerosol Science and Technology, 52, 146–164, https://doi.org/10.1080/02786826.2017.1387229, 2018.